Journal of Ultrafine Grained and Nanostructured Materials
https://jufgnsm.ut.ac.ir
Vol. 56, No.2, December 2023, pp. 205-212
Print ISSN: 2423-6845 Online ISSN: 2423-6837
DOI: 10.22059/jufgnsm.2023.02.09

Glass formation in $Cu_{50}Zr_{50-x}Al_x$ and $(Cu_{50}Zr_{43}Al_7)_{100-x}Nb_x$ alloys

***Majid Tavoosi*[1,*]**

[1]*Department of Materials Engineering, Malek Ashtar University of Technology (MUT), Iran.*

Recieved: 11 November 2023; Accepted: 1 December 2023

**Corresponding author email: ma.tavoosi@gmail.com*

ABSTRACT

In the present work, the effects of Al and Nb elements on the formation of glassy phase in Cu-Zr based bulk metallic glasses (BMGs) have been investigated. In this regards, different $Cu_{50}Zr_{50-x}Al_x$ and $(Cu_{50}Zr_{43}Al_7)_{100-x}Nb_x$ samples with 2 mm in diameter were prepared using arc melting followed by injection casting in water-cooled copper mold. The results illustrated that Al has positive effect on increasing the glass forming ability (GFA) of Cu-Zr system, and it is possible to create a completely glassy structure in $Cu_{50}Zr_{43}Al_7$ sample. In contrast, the addition of Nb has destructive effects on glass forming ability, the homogeneity and final mechanical properties of Cu-Zr-Al BMGs. The segregation of Nb during solidification process and precipitation of brittle B2-CuZr and $Cu_{10}Zr_7$ phases are the main reasons of lower ductility and compressive strength in the presence of Nb element. As-solidified samples containing Nb showed compressive fracture strength in the range of 1000-1650 MPa, which was much lower than Nb-free alloy (2050 MPa).
Keywords: Bulk metallic glass; Injection casting; Cu-Zr-Al; Mechanical properties.

Keywords: *R Bulk metallic glass; Injection casting; Cu-Zr-Al; Mechanical properties.*

1. Introduction

Bulk metallic glasses have attracted much attention due to superior strength, significant elastic strain, and resistance to corrosion and wear compared to conventional crystalline alloys [1-3]. Among the various alloying systems with high glass-forming ability, the Cu-Zr based system is particularly interesting for engineering applications, as it constitutes relatively inexpensive elements. However, the low glass forming ability (GFA) of this alloying system is a limitation for real applications [3-9]. In fact, this system has a lower GFA than BMGs containing Be or Pd, and efforts are ongoing to compensate for this problem.

It is well known that the GFA of Cu-Zr system can increase by adding a third element such as Al, Ti, Ni or Ag to composition. Among all, Cu-Zr-Al alloys have been considered due to their high GFA and superior mechanical properties. Moreover, it has been shown that rare earth elements such as Lu, Y, Nb and Dy rare earths has positive effects on GFA and mechanical properties of Cu-Zr-Al alloy. However, the exact effects of these elements on physical and mechanical properties of Cu-Zr-Al system have not been properly known [9-12].

Despite extensive studies in the field of Cu-Zr based BMGs [8-15], a detailed theoretical study on the reason for choosing Zr as an additive element to Cu-based BMGs and the its optimal percentage has not been properly presented. In addition, the

exact effect of Al and Nb elements on the structural and mechanical properties of Cu-Zr based BMGs has not been evaluated. So, the present work focuses on the investigation about the effect of Al and Nb as the third and fourth component on the formation of glassy phase in $Cu_{50}Zr_{50-x}Al_x$ and $(Cu_{50}Zr_{43}Al_7)_{100-x}Nb_x$ systems. Theoretical investigations (based on the Miedema model [16, 17]) about the effect of different elements on GFA of Cu-Zr based BMGs is another goal of this research.

2. Materials and methods

In the presented work, high purity (≥99.5%) Cu, Zr, Al and Nb elements were used as row materials. $Cu_{50}Zr_{50-x}Al_x$ (x=0, 3.5, 7 at.%) and $(Cu_{50}Zr_{43}Al_7)_{100-x}Nb_x$ (x=1, 3, 5 at.%) ingots were prepared using arc melting method. For the chemical homogeneity, each ingot was melted three times, and finally, cylindrical rods with 2 mm in diameter and 30 mm in length of were prepared using injection casting method in water-cooled copper mold.

The structural characteristics of the samples were investigated using Philips PW3710 X-ray diffraction (XRD) with Cu-Kα radiation at 40 kV (2θ range: 20-80°; step size: 0.05°; time per step 1 s). The microstructural and morphological characterizations of the prepared samples were investigated using transmission electron microscopy (TEM, Jeol-JEM-3010) and scanning electron microscopy (SEM, VEGA-TESCAN-XMU). Mechanical properties of the samples were also determined using Instron testing machine. Uniaxial compression test was performed on as-solidified samples under strain rate of 5×10^{-4} s^{-1} at environment temperature.

3. Results and discussion

Miedema's model is a semi-empirical approach for estimating the heat of formation of solid or liquid metal alloys and compounds in the framework of thermodynamic calculations for metals and minerals. It may provide or confirm basic enthalpy data needed for the calculation of phase diagrams of metals, via CALPHAD or ab initio quantum chemistry methods [16, 17]. In this regard, the mixing enthalpy ($\Delta H^{mix.}$) of various elements to copper (calculated based on the Miedema model) are presented in Table. 1. As can be seen, among all elements introduced in this table, only

Table 1- The mixing enthalpy ($\Delta H^{mix.}$) of various elements to copper calculated based on the Miedema model

element	Pt	Zr	Pd	Al	Ti	Au	Ni	Ag
ΔH^{mix}	-68	-65.76	-59.18	-46.86	-40.6	-39.98	6.21	9.7
element	**Nb**	**V**	**Mn**	**Co**	**Cr**	**Fe**	**Mo**	**W**
ΔH^{mix}	11.7	20.67	14.88	24.98	49.79	51.45	81.3	98.96

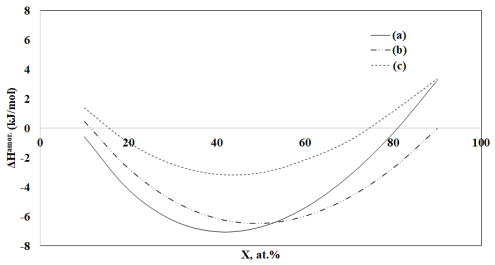

Fig. 1- The formation enthalpy of amorphous phase ($\Delta H^{amor.}$) of a) $Cu_{1-x}Zr_x$, b) $Cu_{1-x}Al_x$ and c) $Cu_{1-x}Ti_x$ systems; calculated based on the Miedema method.

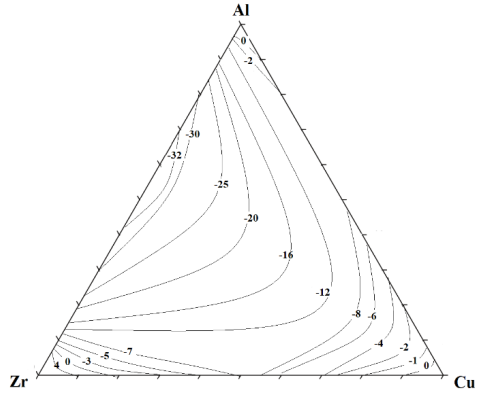

Fig. 2- TThe formation enthalpy of amorphous phase ($\Delta H^{amor.}$) of Cu-Zr-Al ternary system; calculated based on the Miedema method.

the mixing enthalpy of Pt, Zr, Pd, Al, Ti and Au in copper is negative, and therefore these elements can be effective on increasing the GFA of Cu-bases alloys. Of course, Pd, Au and Pt are expensive elements and this limitation makes Cu-Zr, Cu-Al and Cu-Ti systems more attractive for engineering applications. In this regard, the formation enthalpy of amorphous phase ($\Delta H^{amor.}$) of $Cu_{1-x}Zr_x$, $Cu_{1-x}Al_x$ and $Cu_{1-x}Ti_x$ alloying systems are presented in Fig. 1. According to this figure several point can be concluded as:

1. The formation enthalpy of Cu-Zr amorphous phase is more negative than Cu-Al and Cu-Ti systems. In other words, Zr is the best choice for designing the chemical composition Cu-based BMGs.

2. The lowest values of $\Delta H^{amor.}$ in $Cu_{1-x}Zr_x$ system occur in 40<x<50 and alloys containing 40-50 at.% of Zr are recommended for preparing Cu-Zr based BMGs.

3. Aluminum is a suitable choice as the third additive element to further increase in glass forming ability of Cu-Zr system. In this regard, the formation enthalpy of amorphous phase of Cu-Zr-Al ternary system are presented in Fig. 2. In fact, this figure confirms the positive effect of aluminum in increasing GFA of Cu-Zr based BMGs. This result is in agreement with presented results with other researchers about the positive effect of Al on increasing in GFA of Cu-Zr based BMGs [18-21].

To confirm the positive effect of Al on increasing the GFA of Cu-Zr alloying system, the XRD spectra of as-solidified $Cu_{50}Zr_{50-x}Al_x$ (x=0, 3.5, 7) rods are presented in Fig. 3. As can be seen, the addition of Al has a significant effect on increasing GFA in the investigated composition. The XRD pattern of as-solidified $Cu_{50}Zr_{50}$ sample (x=0) consists of several sharp peaks corresponding to B2-CuZr and $Cu_{10}Zr_7$ crystalline phases. The SEM micrograph of this sample in Fig. 4 also confirm the precipitation of blade like crystalline $Cu_{10}Zr_7$ phase with average particle sizes of about 300 nm in matrix. $Cu_{10}Zr_7$ phase belongs to the Aba2 space group and has a Pearson's symbol of oC68, with $Ni_{10}Zr_7$ type structure [18]. In contrast, the XRD pattern

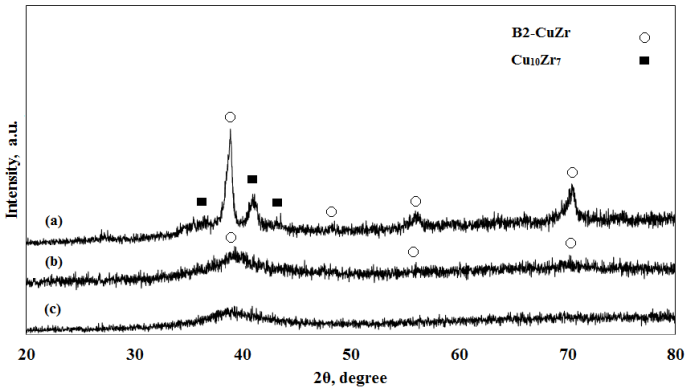

Fig. 3- The XRD patterns of as-solidified $Cu_{50}Zr_{50-x}Al_x$ (x=0, 3.5, 7) rods with 2 mm in diameter; a) x=0, b) x=3.5 and c) x=7.

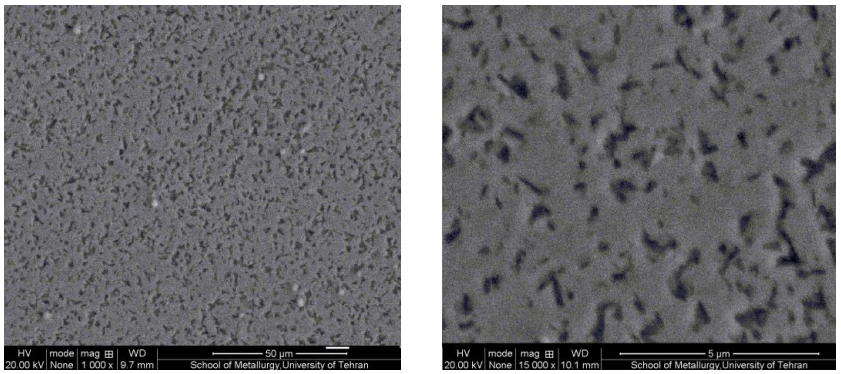

Fig. 4- The SEM micrographs of as-solidified $Cu_{50}Zr_{50}$ rod with 2 mm in diameter at two magnifications.

of $Cu_{50}Zr_{46.5}Al_{3.5}$ as-solidified sample exhibits an amorphous hump and distinguishable B2-CuZr austenite (Pm-3m space group, a=0.3256 nm [18]) crystalline peaks. The SEM micrographs of this sample in Fig. 5 shows the non-uniform distribution of spherical deposits of B2-CuZr in amorphous matrix. As can be seen, the size and distribution of the precipitates formed along the radius of the rod is not uniform and is more refined towards the outer region of the rod due to the higher cooling rate achieved in the injection casting process. It is important to note that, the B2-CuZr phase is unstable and can only be obtained at the certain rate of solidification [13]. As seen in Fig. 3 (c), the XRD pattern of $Cu_{50}Zr_{43}Al_7$ sample only consists of one broad diffuse peak without any evidence of crystalline peaks. The lack of crystalline peaks in this XRD pattern confirms the disordered nature of this sample which is in agreement with the presented TEM image in Fig. 6.

The compression stress-stain curves of as-solidified $Cu_{50}Zr_{50-x}Al_x$ (x=0, 3.5, 7) samples with 2 mm in diameter are presented in Fig. 7. Based on this figure, the maximum strength value in the analyzed samples reaches 2050 MPa in $Cu_{50}Zr_{46.5}Al_{3.5}$ sample. Meanwhile, unlike the other two samples, this composition has shown plastic ductility up to about 2.1%. In other words, among investigated samples, only the $Cu_{50}Zr_{46.5}Al_{3.5}$ alloy showed plastic behavior and other samples broke brittlely during compression test. In fact, the work hardening and plasticity of as-solidified $Cu_{50}Zr_{46.5}Al_{3.5}$ sample can be related to the precipitation of metastable B2-CuZr austenite phase as shown in Fig. 3 (b). This phase transform into a B19′-CuZr martensitic phase with P21/m space group during deformation (deformation-induced phase transformation [18-21]) and causes the sample to show plastic behavior. The presented

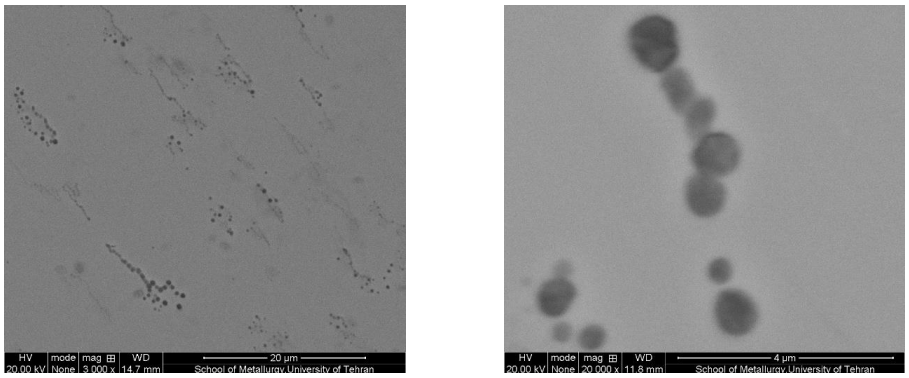

Fig. 4- The SEM micrographs of as-solidified $Cu_{50}Zr_{46.5}Al_{3.5}$ rod with 2 mm in diameter at two magnifications.

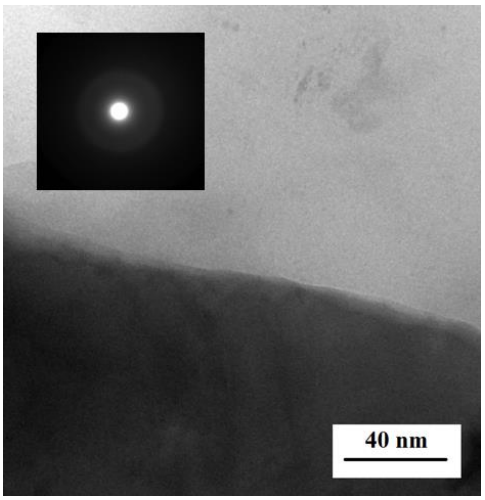

Fig. 6- The TEM image of as-solidified Cu50Zr43Al7 rod with 2-mm in diameter.

results are consistent with the fracture surface SEM micrographs of the samples after compression test in Fig. 8. Based on this figure, all fracture surfaces have vein-like pattern but with different morphologies which can be related to plasticity. In fact, the plasticity of BMGs is highly concentrated in locally deformed shear bands (SBs), while a rapid expansion of a SB leads to catastrophic failure, but the interaction between multiple SBs reduces the rapid expansion of SBs, thereby improving the plasticity of the BMGs [19]. In contrast, the characteristics of the vein-like pattern are related to the plasticity and strength of BMGs. A high density and smaller size of the vein-like patterns indicate fairly good plasticity and strength of the BMGs [20]. From the Fig. 8, it can be observed that there are many SBs

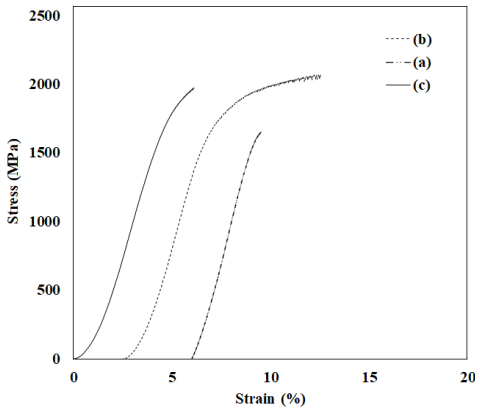

Fig. 7- The compression true stress-stain curves of as-solidified $Cu_{50}Zr_{50-x}Al_x$ (x=0, 3.5, 7) rods with 2 mm in diameter; a) x=0, b) x=3.5 and c) x=7.

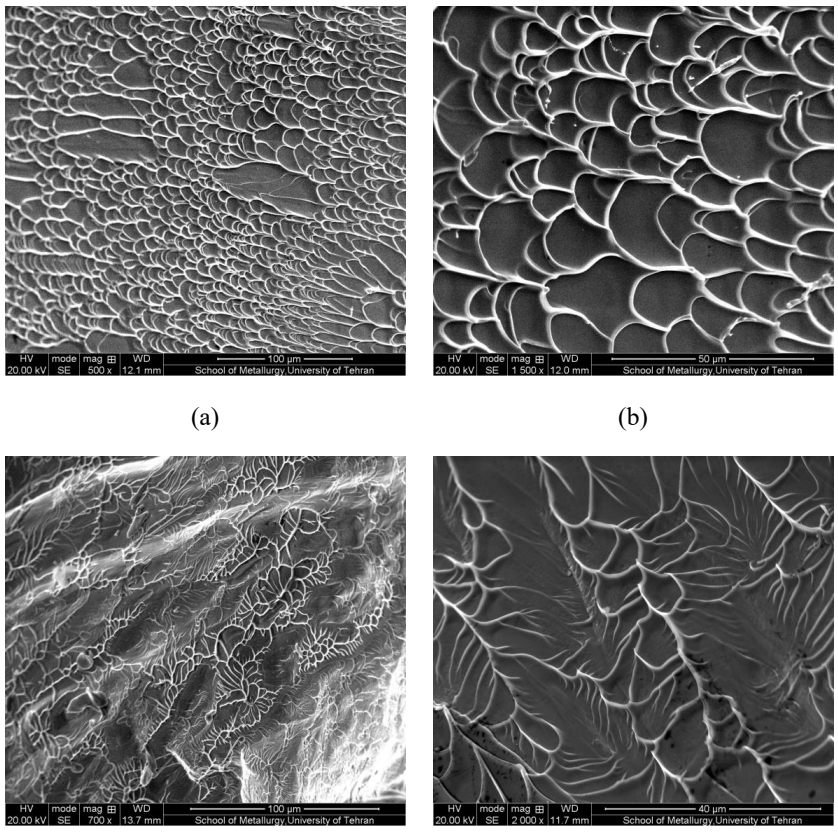

Fig. 8- The SEM fractured surface morphologies of as-solidified $Cu_{50}Zr_{50-x}Al_x$ rods; a-b) x=0, c-d) x=3.5.

on $Cu_{50}Zr_{46.5}Al_{3.5}$ (x=3.5) alloy, and the interaction between SBs inhibits the rapid expansion of SBs, thus its plasticity is improved. In contrast, $Cu_{50}Zr_{50}$ (x=0) alloy has the least level of SBs, so its plasticity is lower than $Cu_{50}Zr_{46.5}Al_{3.5}$ (x=3.5).

It has been found that rare earth elements can have a positive effect on increasing the ability to form the glass phase in Cu-Zr-Al alloys. In this re-

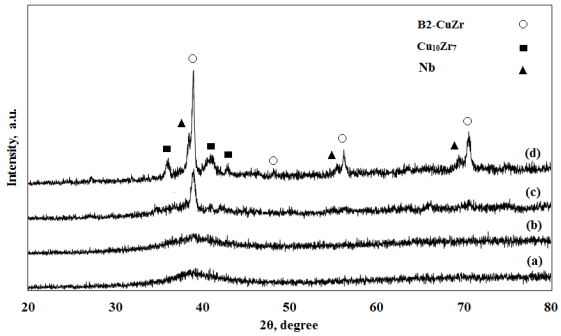

Fig. 9- The XRD patterns of as-solidified $(Cu_{50}Zr_{43}Al_7)_{100-x}Nb_x$ (x=0, 1, 3, 5) rods (with 2-mm in diameter); a) x=0, b) x=1, c) x=3 and d) x=5.

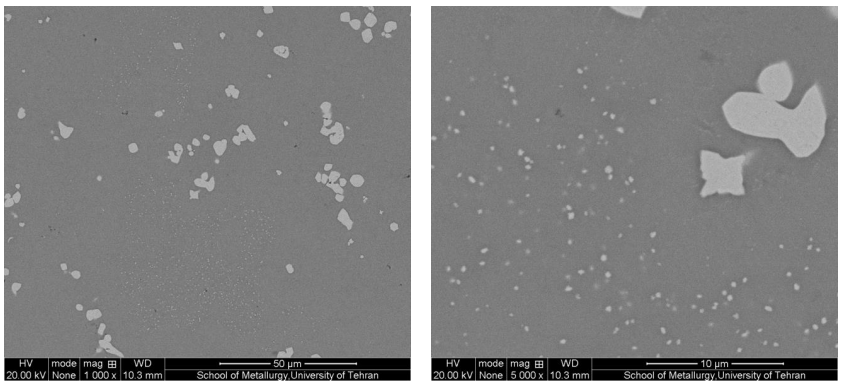

(a) (b)

Fig. 10- The SEM micrographs of as-solidified $(Cu_{50}Zr_{43}Al_7)_{95}Nb_5$ rod (in two magnifications).

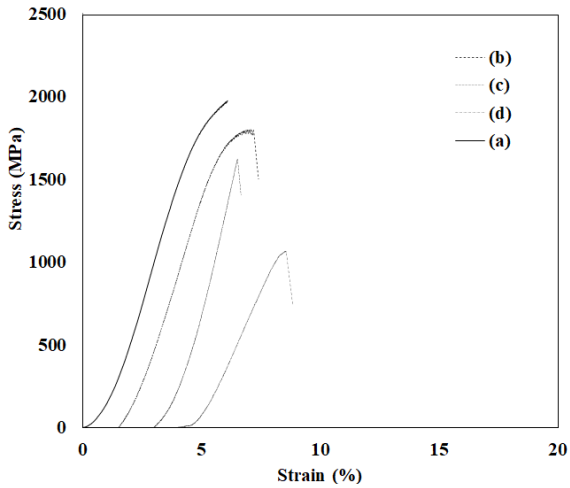

Fig. 11- The compression true stress-stain curves of as-solidified (Cu50Zr43Al7)100-xNbx (x=0, 1, 3, 5) rods (with 2-mm in diameter); a) x=0, b) x=1, c) x=3 and d) x=5.

search, Nb was selected as an additive element of $Cu_{50}Zr_{43}Al_7$ alloy. The XRD patterns of as-solidified $(Cu_{50}Zr_{43}Al_7)_{100-x}Nb_x$ (x=0, 1, 3, 5) rods with 2-mm in diameter are displayed in Fig. 9. As can be seen, a broad diffraction halo without detectable crystalline peaks are main characteristics of corresponding XRD patterns to x≤1. In contrast, the presented XRD patterns in Fig. 9 (c) & (d) revels that, the structure of as-solidified samples with x>1 compose of B2-CuZr, $Cu_{10}Zr_7$ and Nb-rich crystalline phases. However, the precipitation of Nb-rich phase in presented XRD patterns (which is in agreement with presented SEM micrographs in Fig. 10) confirm the tendency of Nb element to segregation during solidification. In fact, the segregation of Nb, has destructive effects on glass forming ability of Cu-Zr-Al system and has led to the precipitation of unwanted phases during solidification. In other word, the Nb had a negative effect on the formation of the glassy phase in the investigated composition.

The stress-strain curves of rapid-solidified $(Cu_{50}Zr_{43}Al_7)_{100-x}Nb_x$ (0, 1, 3, 5) samples are presented in Fig. 11. As seen, all Nb-containing samples show lower compressive fracture strength (1000-1650 MPa) in comparison with $Cu_{50}Zr_{43}Al_7$ BMG (1980 MPa). The SEM micrographs of lateral fracture and fracture surface morphology of $(Cu_{50}Zr_{43}Al_7)_{99}Nb_1$ sample are shown in Fig. 12. Based on this figure, the fracture surface of this sample includes a fully developed vein-like pattern that is known as a characteristic in monolithic BMGs [14]. As seen, this sample fractures catastrophically along one dominates shear plane, which are visible on the lateral surface (The fracture angle of 45°). These evidences justify the lack of plasticity in these samples. In fact, the segregation of Nb during solidification process and precipitation of brittle B2-CuZr and $Cu_{10}Zr_7$ phases are the main reasons of lower ductility and compressive strength in the presence of Nb element. In other word, the addition of Nb has destructive effects on glass forming ability, the homogeneity and final mechanical properties of Cu-Zr-Al BMGs.

4. Conclusion

In this work, the effect of Al and Nb on the formation of glassy phase in $Cu_{50}Zr_{50-x}Al_x$ and $(Cu_{50}Zr_{43}Al_7)_{100-x}Nb_x$ systems were evaluated. The results illustrated that;

1. Al has a positive effect on increasing the glass forming ability (GFA) of Cu-Zr system, and it is possible to create a completely glassy structure in $Cu_{50}Zr_{43}Al_7$ sample.

2. The maximum strength value in $Cu_{50}Zr_{50-x}Al_x$ samples reaches 2050 MPa in the x=3.5 combination. Meanwhile, unlike the other samples, this composition has shown plastic ductility up to about 2.1% as a result of precipitation of metastable B2-CuZr during solidification.

3. In contrast to Al, Nb has a destructive effect on glass forming ability of $Cu_{50}Zr_{43}Al_7$ based bulk metallic glasses. This element has a great tendency to separate and form Nb-rich phases, which causes a sharp decrease in the final mechanical properties.

4. As-solidified samples containing Nb showed compressive fracture strength in the range of 1000-1650 MPa, which was much lower than compressive strength of Nb-free alloy.

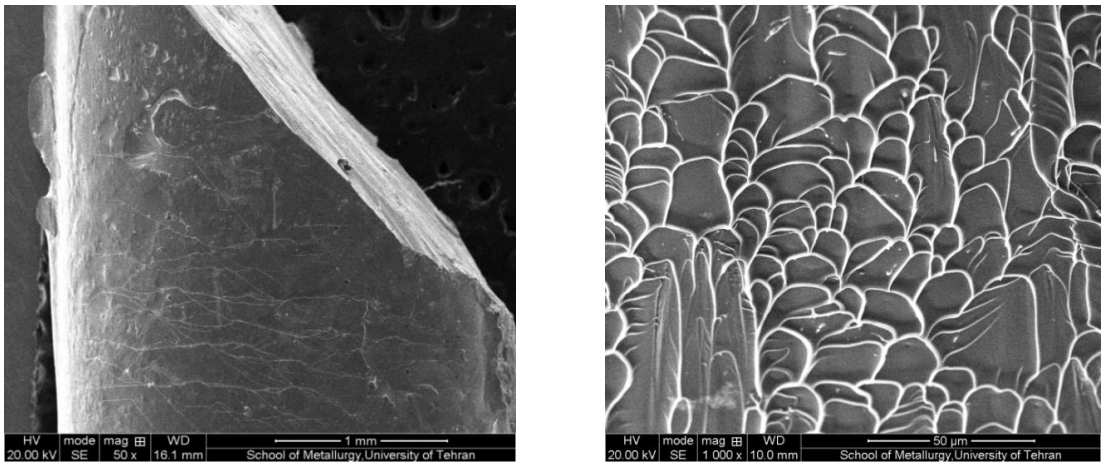

Fig. 12- The SEM micrographs of a) lateral and b) fracture surface of rapid-solidified $(Cu_{50}Zr_{43}Al_7)_{99}Nb_1$ sample.

References

1. Inoue A, Takeuchi A. Recent development and application products of bulk glassy alloys. Acta Materialia. 2011;59(6):2243-67.
2. Inoue A. Stabilization of metallic supercooled liquid and bulk amorphous alloys. Acta Materialia. 2000;48(1):279-306.
3. Zhou K, Liu Y, Pang S, Zhang T. Formation and properties of centimeter-size Zr–Ti–Cu–Al–Y bulk metallic glasses as potential biomaterials. Journal of Alloys and Compounds. 2016;656:389-94.
4. Tam MK, Pang SJ, Shek CH. Corrosion behavior and glass-forming ability of Cu–Zr–Al–Nb alloys. Journal of Non-Crystalline Solids. 2007;353(32-40):3596-9.
5. Trexler MM, Thadhani NN. Mechanical properties of bulk metallic glasses. Progress in Materials Science. 2010;55(8):759-839.
6. Ding J, Inoue A, Zhu SL, Wu SL, Shalaan E, Al-Ghamdi AA. Formation, microstructure and mechanical properties of ductile Zr-rich Zr–Cu–Al bulk metallic glass composites. Journal of Materials Research and Technology. 2021;15:5452-65.
7. Yang YJ, Cheng BY, Lv JW, Li B, Ma MZ, Zhang XY, et al. Effect of Ag substitution for Ti on glass-forming ability, thermal stability and mechanical properties of Zr-based bulk metallic glasses. Materials Science and Engineering: A. 2019;746:229-38.
8. Zhang Y, Yao J, Zhao X, Ma L. Ti substituted Ni-free $Zr_{65-x}Ti_{x}Cu_{17.5}Fe_{10}Al_{7.5}$ bulk metallic glasses with significantly enhanced glass-forming ability and mechanical properties. Journal of Alloys and Compounds. 2019;773:713-8.
9. Cao D, Wu Y, Liu XJ, Wang H, Wang XZ, Lu ZP. Enhancement of glass-forming ability and plasticity via alloying the elements having positive heat of mixing with Cu in Cu48Zr48Al4 bulk metallic glass. Journal of Alloys and Compounds. 2019;777:382-91.
10. Lu Y, Huang G, Qin Z, Lu X, Huang Y. Mössbauer study of the ultrahigh glass-forming ability in FeCoCrMoCBY alloy system. Vacuum. 2017;141:173-5.
11. Sengul S, Celtek M, Domekeli U. Molecular dynamics simulations of glass formation and atomic structures in $Zr_{60}Cu_{20}Fe_{20}$ ternary bulk metallic alloy. Vacuum. 2017;136:20-7.
12. Li H, Lu Y, Qin Z, Lu X. Vibrational properties of FeCoCrMoCBY bulk metallic glasses and their correlation with glass-forming ability. Vacuum. 2016;133:105-7.
13. Chen J, Zhang Y, He J, Yao K, Wei B, Chen G. Metallographic analysis of Cu–Zr–Al bulk amorphous alloys with yttrium addition. Scripta Materialia. 2006;54(7):1351-5.
14. Suryanarayana C, Inoue A. Bulk metallic glasses. CRC press; 2017 Nov 22.
15. Wang W. Roles of minor additions in formation and properties of bulk metallic glasses. Progress in Materials Science. 2007;52(4):540-96.
16. Miedema AR, de Boer FR, Boom R. Model predictions for the enthalpy of formation of transition metal alloys. Calphad. 1977;1(4):341-59.
17. Das N, Mittra J, Murty BS, Pabi SK, Kulkarni UD, Dey GK. Miedema model based methodology to predict amorphous-forming-composition range in binary and ternary systems. Journal of Alloys and Compounds. 2013;550:483-95.
18. Deng L, Zhou B, Yang H, Jiang X, Jiang B, Zhang X. Roles of minor rare-earth elements addition in formation and properties of Cu–Zr–Al bulk metallic glasses. Journal of Alloys and Compounds. 2015;632:429-34.
19. Xie Z, Zhang Y, Yang Y, Chen X, Tao P. Effects of rare-earth elements on the glass-forming ability and mechanical properties of $Cu_{46}Zr_{47-x}Al_{7}M_{x}$ (M = Ce, Pr, Tb, and Gd) bulk metallic glasses. Rare Metals. 2010;29(5):444-50.
20. Fu J, Men H, Pang S, Ma C, Zhang T. Formation and thermal stability of Cu-Zr-Al-Er bulk metallic glasses with high glass-forming ability. Journal of University of Science and Technology Beijing, Mineral, Metallurgy, Material. 2007;14:36-8.